Enhanced thermoelectric performance of $Mg_2Si_{1-x}Sn_x$ codoped with Bi and Cr

Vikram,[1] Duane D. Johnson,[2,3] and Aftab Alam[1,*]

[1]*Department of Physics, Indian Institute of Technology, Bombay, Powai, Mumbai 400 076, India*

[2]*Department of Materials Science and Engineering, Iowa State University, Ames, Iowa 50011, USA*

[3]*Division of Materials Science and Engineering, Ames Laboratory, Ames, Iowa 50011, USA*

(Received 18 July 2018; published 21 September 2018)

Magnesium silicides are favorable thermoelectric materials considering resource abundance and cost. Chromium (Cr) doping in magnesium silicides has not yet been explored. Using first-principles calculations, we have studied the stability of Mg_2Si with chromium (1.85, 3.7, 5.55, and 6.25% Cr) and tin (12.5 and 50% Sn). Three Mg_2Si compounds doped with Sn, (Sn + Bi), and (Sn + Bi + Cr) are used to explain doping effects on thermoelectric performance. Notably, Cr behaves nonmagnetically for $\leqslant$2% Cr, after which ferromagnetic ordering is favored ($\leqslant$12.96% Cr), despite its elemental antiferromagnetic state. With alloying of Sn (70.4%), Mg_2Si remains an indirect-band-gap semiconductor, but adding small amounts of Bi (3.7%) increases the carrier concentration such that electrons occupy conduction bands, making it a degenerate semiconductor. $Mg_2Si_{0.296}Sn_{0.666}Bi_{0.037}$ is found to give the highest thermoelectric figure of merit (ZT) and power factor (PF) at 700 K, i.e., 1.75 and 7.04 mW m^{-1} K^{-2}, respectively. Adding small %Cr decreases ZT and PF to 0.78 and 4.33 mW m^{-1} K^{-2}, respectively. Such a degradation in thermoelectric (TE) performance is attributed to two factors: (i) uniform doping acting as an electron acceptor, decreasing conduction, and (ii) the loss of low-lying conduction band degeneracy with doping, decreasing the Seebeck coefficients. A study of configurations of Cr doping suggests that Cr has a tendency to form clusters inside the lattice, which play a crucial role in tuning the magnetic and TE performance of doped Mg_2Si compounds.

DOI: 10.1103/PhysRevB.98.115204

I. INTRODUCTION

Energy demand is a considerable global concern and it continues to grow. Among energy-conversion technologies, thermoelectricity (TE) continues gaining attention because of the direct conversion of heat into electrical energy. Also, TE devices do not involve moving parts, so they are easier to fabricate and are free from noise pollution.

Metals were used for early TE applications due to their good electrical conductivity, but the TE figure of merits [ZT values, see Eq. (1)] were low due to their high thermal conductivities. Hence, for band-structure engineering, research developed on doping and alloying to tune thermal and electrical transport to maximize ZT. Today, a few of the most popular TE materials are Bi_2Te_3, $Si_{1-x}Ge_x$ and PbTe with ZT > 1, where ZT > 2 would be commercially competitive among state-of-the-art TE materials [1–3]. Other bulk materials, such as complex chalcogenides [4,5], skutterudites [6,7], and quasicrystals [8], also show potential for TE applications.

Mg_2Si stands out from all thermoelectric materials due to its advantage of being synthesized from cheap, abundant, and eco-friendly raw materials, possessing high output power per mass unit and offering great potential for efficient TE performance [9–12]. For pure Mg_2Si, depending upon the synthesis technique, the ZT values are found to range from 0.1 to 0.4 [13]. Efforts have been made to enhance the thermoelectric performance using the effects of doping, thin films, nanostructuring, and nanoparticle additions into bulk matrix. Bidoped Mg_2Si semiconductors yield a ZT of 0.86 at 862 K for 2% Bi in place of Si [14], whereas small amounts of Sb (<2.5%) increase the conductivity with small decreases in Seebeck coefficients due to additional charge carriers [15]. With precipitate formation for small amounts of Sb in Mg_2Si, a decrease in thermal conductivity has been observed from point defect and interface scattering. The best ZT value thus far is 0.65 at 873 K for 2% Sb doping [15].

Small amounts of Sn reduce the band gap and give smaller lattice thermal conductivity. ZT > 1.45 at 750 K is reported for a combined optimal Sn, Sb, and Ge doping for Si in Mg_2Si [16]. Solid solutions of Mg_2 (Si, Sn) with nanoparticles and (unavoidable) segregated phases were formed [17] with a maximum ZT of 0.9. At optimal Sn doping in Mg_2Si [9], ZT as high as 1.1 is reported, comparable to the best PbTe and *n*-SiGe alloys. TiO_2 nanoparticles are found to increase the thermoelectric efficiency when added in small amounts in pure and Sn-doped Mg_2Si [17–20]. Even (110) surface thin films of Mg_2Si are found to enhance the Seebeck coefficient over that of bulk [19]. In all, Mg_2Si serves as a very promising and economical TE material with suitable doping and nanostructuring [21]. Transition-metal doping in Mg_2Si has not yet been studied in regards to TE performance. However, a few reports exist for Cr doped in $MnSi_2$, where Cr is found to increase the electrical conductivity [22,23]. This also results in a small decrease in Seebeck coefficients, thereby decreasing ZT [23].

Here we have performed detailed first-principles calculations of combined Sn alloying in Mg_2Si with codoping of

*aftab@phy.iitb.ac.in

Bi and Cr. The calculations address the stability, electronic structure, and thermoelectric properties, including ZT. Various magnetic and structural Cr configuration at different levels of Cr are simulated and a tendency for Cr clustering in the lattice is found favorable. Alloying with Sn reduces the band gap (but it remains indirect), whereas small amounts of Bi increase the carrier concentration and make Mg_2Si a degenerate semiconductor. Combined doping, such as $Mg_2Si_{0.296}Sn_{0.666}Bi_{0.037}$, yields a high power factor (PF; 7.04 mW m^{-1} K^{-2}) and the highest ZT (1.75). A small amount of Cr causes a reduction in ZT to 0.78 at 700 K, attributed to the decrease in Seebeck coefficient and electrical conductivity (Cr acts as electron acceptor).

One of the main goals of the present work is to make accurate prediction of band-gap-related properties for a better comparison with future experiments on these systems. Local density or generalized-gradient-approximation exchange-correlation functionals are known to underestimate drastically the band gap. Hybrid functional (HSE06), however, usually predicts band gaps comparable to experiments. As such, we have used the HSE06 functional to simulate the band properties of all the system investigated here.

II. COMPUTATIONAL DETAILS

We employ first-principles simulations using density functional theory (DFT) [24] as implemented in Vienna *ab initio* simulation package (VASP) [25–27] with a projected augmented-wave basis [28] and the generalized gradient approximation (GGA) exchange-correlation functional of Perdew, Burke, and Ernzerhof (PBE) [29]. For more reliable estimates of the band gap, a hybrid functional (HSE06) [30] is used for all the systems and reveals shortcomings of some GGA-PBE results. A plane wave cutoff of 500 eV was used in all calculations. The Brillouin zone sampling was done by using Γ-centered k-point mesh; e.g., for ordered Mg_2Si, meshes of $12 \times 12 \times 12$ (ionic relaxations) and $20 \times 20 \times 20$ [self-consistent field (scf) solutions] were used. Cell volume, shape, and atomic positions for all the structures were fully relaxed using conjugate gradient algorithms until the forces on each atom was below 0.001 eV/Å. The total energy was converged to 10^{-5} eV. The tetrahedron method with Blöchl corrections [31] was used to calculate the electronic density of states. To study various Cr-doping and Sn-alloying concentrations, $3 \times 3 \times 3$ and $2 \times 2 \times 2$ supercell geometries were used. The percentage of doping or alloying is dictated by the number of atoms replacing the host Mg or Si atoms in the supercell. For a $3 \times 3 \times 3$ supercell, Γ-point relaxation was used with a $4 \times 4 \times 4$ mesh for scf charges. For a $2 \times 2 \times 2$ supercell, $6 \times 6 \times 6$ and $10 \times 10 \times 10$ meshes were used for relaxation and scf calculations, respectively.

For a given absolute temperature T, the conversion efficiency of a thermoelectric (TE) device depends upon the transport coefficients of the constituent material through the following dimensionless figure of merit (ZT) as

$$ZT = \frac{S^2\sigma}{\kappa_e + \kappa_L} T, \tag{1}$$

where S is the Seebeck coefficient, σ is the electrical conductivity, and κ_e and κ_L are the thermal conductivity due to electrons and phonons, respectively. As a TE figure of merit, higher values of ZT correlate with better efficiency. The main challenge is to enhance ZT, as the transport parameters S, σ, and κ (κ_e and κ_L) are related to each other and primarily depend upon the electronic structure, carrier concentration, and other system-dependent properties. For instance, the electronic thermal conductivity and electrical conductivity are related to each other by the Wiedemann-Franz law,

$$\kappa_e = L\sigma T, \tag{2}$$

where L is the Lorenz number. This relation clearly shows that increasing σ also increases κ_e.

We use the BoltzTraP code [32] to estimate the TE properties of $Mg_2Si_{0.296}Sn_{0.704}$, $Mg_2Si_{0.296}Sn_{0.666}Bi_{0.037}$, and $Mg_{1.981}Cr_{0.019}Si_{0.296}Sn_{0.666}Bi_{0.037}$. In this code, the semiclassical Boltzmann transport formalism is used with a constant relaxation time approximation (cRTA) to determine the Seebeck coefficient (S) and electrical conductivity (σ). The κ_e was obtained from Eq. (2) with L estimated [33] as

$$L = 1.5 + e^{-|S|/116}, \tag{3}$$

where $|S|$ is the absolute values of Seebeck coefficient in units of μVK^{-1}. Accurate calculations from the BoltzTraP code require calculations on a dense k-point mesh. For $3 \times 3 \times 3$ supercell geometries, $10 \times 10 \times 10$ mesh was used to perform non-self-consistent field calculations from preconverged charge densities and the k-mesh was further enhanced (10 times) by interpolation to calculate the transport properties.

In the cRTA, BoltzTraP calculates transport with a constant carrier relaxation time (τ) in which properties like conductivity (σ) are scaled as σ/τ. The appropriate values of relaxation time are evaluated by comparing the theoretical (σ/τ) values at a particular temperature (T) and carrier concentration (n) with the experimentally reported values of σ at those T and n. These τ values are then used to obtain the desired σ values. The obtained carrier relaxation time (τ) and the lattice thermal conductivity taken from experimental data [34] are given in the Supplemental Material [35] (see Sec. I and Fig. S1).

Mg_2Si has an antifluorite structure with space group $Fm\bar{3}m$ (no. 225); see Fig. 1. With a being the lattice parameter, structural optimization gives the most stable structure with Wyckoff positions for Mg at 8c sites [$a(\frac{1}{4}, \frac{1}{4}, \frac{1}{4})$ and $a(\frac{3}{4}, \frac{3}{4}, \frac{3}{4})$] and Si at 4$a$ sites [a(0,0,0)]. The band structures are plotted along the high-symmetry direction in the Brillouin zone; see Fig. 1.

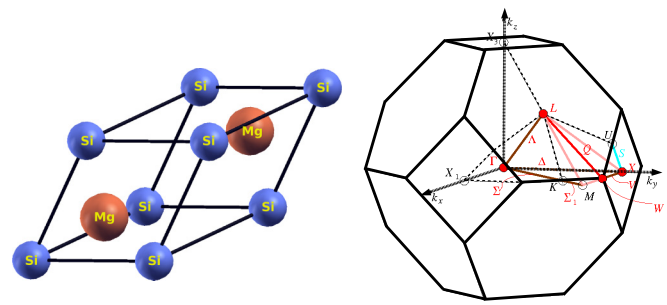

FIG. 1. Primitive cell of Mg_2Si (left) and its first Brillouin zone (right) showing the high-symmetry lines.

Formation energy (ΔE_f) of any compound is the energy cost or gain for the formation of the compound from its constituent elements. Here, ΔE_f for Cr-doped, Sn-alloyed system $Mg_{2-x}Cr_xSi_{1-y}Sn_y$ is calculated as

$$\Delta E_f = E(Mg_{2-x}Cr_xSi_{1-y}Sn_y) - [(2-x)E^{Mg} + xE^{Cr} + (1-y)E^{Si} + yE^{Sn}] \quad (4)$$

from the total energy E of the corresponding compound (element) in its equilibrium phase. A negative (positive) value of the ΔE_f signifies increased (decreased) stability relative to its constituent elements.

III. RESULTS AND DISCUSSION

A. Stability and electronic structure

Before calculating the TE properties, we first evaluate the stability of the alloyed Mg_2Si, including Cr (1.85%, 3.7%, 5.55%, and 6.25%), Sn (11.11% and 48.15%), and combined Cr+Sn compounds. Table I shows ΔE_f for various amounts of Cr and Sn in Mg_2Si. Pure Mg_2Si is found to be the most stable, and it slowly decreases as Cr increases. The configurations where Cr atoms are placed near to each other are more stable compared to those where they are placed far apart. In the table, subscript labels 1 and 2 denote configurations where Sn atoms are placed near or far from each other, respectively. The lower ΔE_f for the Sn_1 atoms suggest that Sn atoms favor being apart from one another; that is, Sn atoms prefer to be uniformly distributed in a sample rather than forming precipitates. The increased amounts of Cr and Sn in the lattice at Mg and Si sites, respectively, make the system less stable. However, the sufficiently high negative values of the formation energy for all the configurations suggests that all compounds are chemically stable. Because the percentage of Bi is a small quantity, its effect on formation energy is very small and hence not shown here.

TABLE I. ΔE_f (meV/atom) for Cr and Sn in $Mg_{2-x}Cr_xSi_{1-y}Sn_y$; "near" ("far") signifies that the atoms are near (far) in the lattice. This effect for Sn are checked for 48.15% Sn given by Sn_1 and Sn_2, respectively.

S. no.	Doping configuration	Formation energy (meV/atom)
1	Pure Mg_2Si	–160.26
2	1.85%Cr	–128.04
3	1.85%Cr + 11.11%Sn	–123.24
4	1.85%Cr + 48.15%Sn	–119.66
5	3.7%Cr_far	–126.72
6	3.7%Cr_far + 11.11%Sn	–122.84
7	3.7%Cr_far + 48.15%Sn_1	–120.06
8	3.7%Cr_far + 48.15%Sn_2	–121.49
9	3.7%Cr_near	–128.53
10	3.7%Cr_near + 11.11%Sn	–124.49
11	3.7%Cr_near + 48.15%Sn_1	–122.60
12	3.7%Cr_near + 48.15%Sn_2	–122.99
13	5.55%Cr_far	–108.70
14	5.55%Cr_far + 11.11%Sn	–105.79
15	5.55%Cr_far + 48.15%Sn	–104.50
16	5.55%Cr_near	–114.89
17	5.55%Cr_near + 11.11%Sn	–109.78
18	5.55%Cr_near + 48.15%Sn	–107.33
19	6.25%Cr	–107.82
20	6.25%Cr + 12.5%Sn	–100.78
21	6.25%Cr + 50%Sn	–97.62

TABLE II. Calculated band cap for pure Mg_2Si obtained by using various exchange-correlation functional.

S. no.	Ex. correlation functional	Band gap (eV)
1	PBE	0.22
2	PBEsol	0.20
3	MetaGGA	0.57
4	PBE0	1.20
5	HSE03	0.46
6	HSE06	0.59

Calculations are performed to study the band dispersion, density of states (DOS), and gaps of pure Mg_2Si and its alloys ($Mg_{2-x}Cr_xSi_{1-y-z}Sn_yBi_z$). As is well known, accurate prediction of band gaps in these systems is challenging. Various experiments have reported band gap of Mg_2Si to be in the range of 0.69–0.78 eV [13]. As noted already, simple GGA-PBE functionals are inaccurate, in general. We have simulated the band gap of Mg_2Si using various functionals, see Table II, where HSE06 and meta-GGA predicted band gaps closest to experiment. However, meta-GGA is not suited for higher throughput band-energy calculations. As such, HSE06 is used for calculating band properties for Mg_2Si-based compounds.

Figure 2 shows the band structure of Mg_2Si using PBE and HSE06 functional. Both functionals predict Mg_2Si to be an indirect gap semiconductor; however, the band gap from HSE06 (0.59 eV) is in better agreement with experimental results [13] than is PBE (0.22 eV). The bands near valence band maxima (VBM) are composed mostly of Si p orbitals, whereas the Mg s orbitals mostly contribute to the bands near conduction band minima (CBM). Figure 2 shows the atom-projected density of states (DOS) using PBE functional. Evidently there is major contribution of Si p orbitals at VBM, whereas Mg s orbitals contribute to the sharp rise of DOS at CBM. Such a rise of DOS at E_F (or flat dispersion near E_F) is desirable feature for better thermoelectric properties. This essentially offers higher effective mass, resulting in higher Seebeck coefficients.

Comparing the PBE and the HSE06 band structure, it is evident (apart from size of the band gaps) that the topology of the bands are almost the same. As is well known, the TE properties depends on the band gap and the band topology. So, to study the TE properties of $Mg_{2-x}Cr_xSi_{1-y-z}Sn_yBi_z$ to a reasonable accuracy, first the simple PBE functional is used to obtain the band structure, and then the HSE06 functional is employed to get a more accurate band gap. The PBE conduction bands are then rigidly shifted to match the HSE06 gap. This rigid-band procedure is often used in calculation of TE properties, and justified due to the close similarity of the topology of bands from PBE and HSE06.

Because valence bands have major contribution from the Si orbitals and conduction bands from Mg orbitals, any doping in place of the Mg site is expected to change the conduction band topology, whereas alloying at the Si site will change

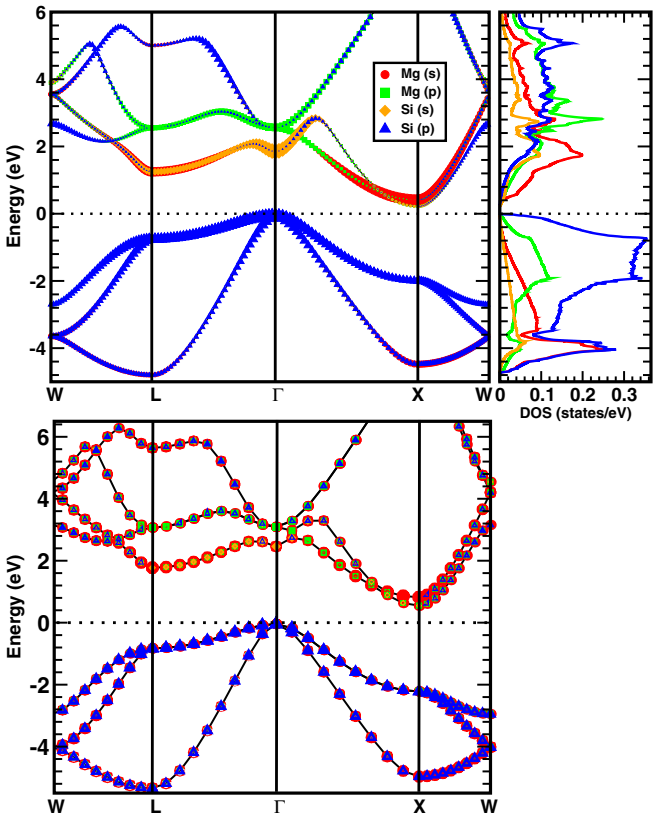

FIG. 2. (top) PBE electronic dispersion with orbital character (left) and atom-projected density of states (DOS) (right) and (bottom) HSE06 dispersion. Orbital contribution of individual atoms is given by colored symbols. The Fermi energy is given by the dashed line.

the valence bands. Figure 3 shows the PBE band structure of $Mg_2Si_{0.296}Sn_{0.704}$ (top), $Mg_2Si_{0.296}Sn_{0.666}Bi_{0.037}$ (middle), and $Mg_{1.981}Cr_{0.019}Si_{0.296}Sn_{0.666}Bi_{0.037}$ (bottom), where the gap in each case is scaled to the HSE06 values. The HSE06 dispersion on a sparse set of k points is shown in the Supplemental Material [35] (see Figs. S2, S3, and S4). As expected, Sn alloying contributes mainly to the valence bands. A small contribution from Sn is visible in conduction bands also, but a majority arise from Mg. As Sn has a similar bonding nature as Si, Mg_2(Si, Sn) remains semiconducting with a reduced band gap.

Interestingly, addition of Bi does not affect the band topology much (see Fig. 3). It neither contributes significantly to the conduction nor to the valence band edges. Bi has major contributions at very low-lying energies, as evident in Fig. S5 [35]. As Bi has an extra electron, it increase the number of charge carriers, causing a shift in the Fermi energy and pushes the extra electron to some conduction bands which were previously empty. Thus, the Bi doping makes the compound a degenerate semiconductor. On the other hand, the addition of Cr in place of Mg, although not affecting the valence bands much, causes various new states to arise near the conduction band edges. This major change in the conduction bands is attributed to the lifting of degeneracy of low-lying conduction bands. The compound remains degenerate semiconductor with Cr doping.

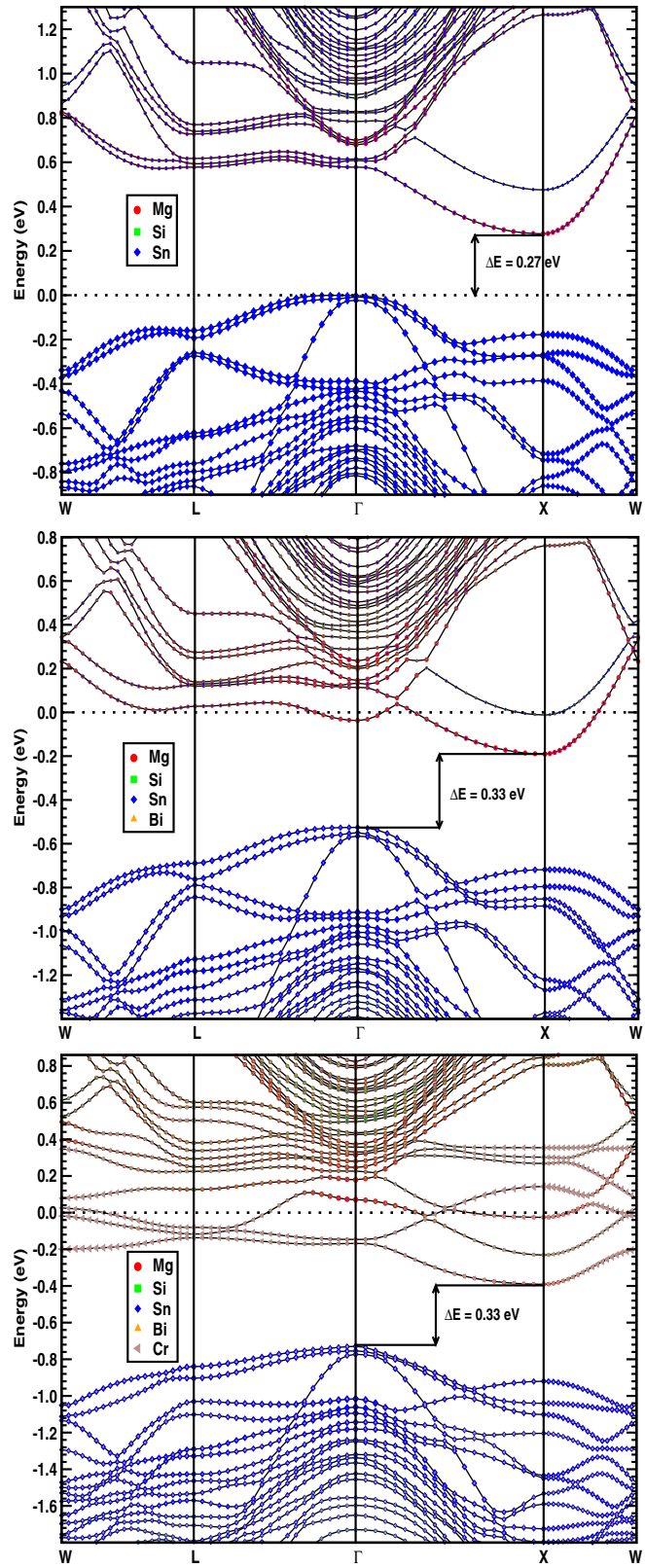

FIG. 3. PBE electronic structure of (top) $Mg_2Si_{0.296}Sn_{0.704}$; (middle) $Mg_2Si_{0.296}Sn_{0.666}Bi_{0.037}$; and (bottom) $Mg_{1.981}Cr_{0.019}Si_{0.296}Sn_{0.666}Bi_{0.037}$. Various atomic contributions are shown by different color symbols. Band gap is scaled to the gap value obtained from HSE06 calculations. The dashed line indicates the Fermi energy.

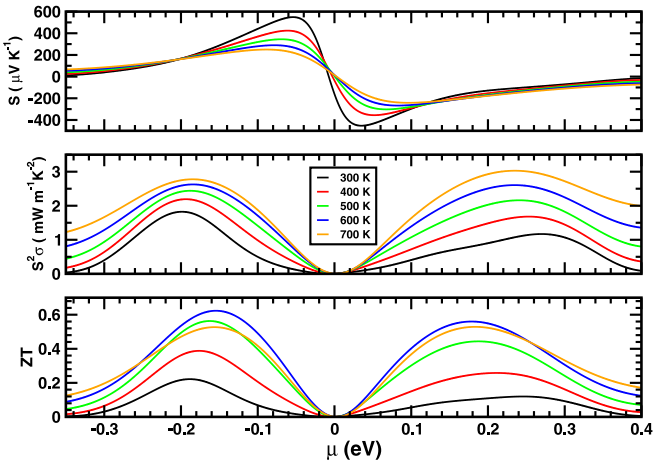

FIG. 4. Seebeck coefficient (S), power factor ($S^2\sigma$), and ZT vs chemical potential μ at T's for $Mg_2Si_{0.296}Sn_{0.704}$.

B. Thermoelectric properties

Here we have studied the effect of Sn, Bi, and Cr doping on Mg_2Si with the help of three representative compounds, namely, $Mg_2Si_{0.296}Sn_{0.704}$, $Mg_2Si_{0.296}Sn_{0.666}Bi_{0.037}$, and $Mg_{1.981}Cr_{0.019}Si_{0.296}Sn_{0.666}Bi_{0.037}$. The experimentally reported doping of Sn in Mg_2Si with optimal thermoelectric performance varies in the range 60–70% [36,37]. We have used 70.4% Sn alloying at the Si site to start with. The motivation behind choosing a small concentration of Bi doping is to induce charge carriers into the lattice [14], thus enhancing the electrical conductivity. Finally, a small amount of Cr is introduced to study its effects on the TE properties.

As explained in Sec. II, the carrier relaxation time (τ) for first two samples were obtained to be 8.26 and 9.80 fs, respectively (see Sec. I of the Supplemental Material [35]). Looking at the τ values of Sn- and (Sn + Bi)-doped samples, a carrier relaxation time of 10 fs is used for Cr-doped compound, keeping in mind the unavailability of any experimental data in this case.

Figure 4 shows the chemical potential (μ) dependence of the Seebeck coefficient (S), power factor ($S^2\sigma$), and ZT at five different temperatures between 300 and 700 K for $Mg_2Si_{0.296}Sn_{0.704}$. The zero chemical potential signifies the center of the band gap. Any movement of μ upward toward the conduction band minima (CBM) or downward toward the valence band maxima (VBM) can be thought of as an increase in n-type or p-type charge carriers. Thus, the carrier concentration increases as we move away from the zero chemical potential line. Seebeck coefficients are negative for n-type charge carriers and positive for p-type charge carriers.

As evident from Fig. 4, an increase in Seebeck coefficient is observed with small increase in μ. Further increase in μ causes a reduction and hence saturation of S. Each μ value corresponds to a unique carrier concentration. Seebeck coefficient attains a maximum value of $-453.09\,\mu VK^{-1}$ for n-type carrier at a chemical potential of 0.04 eV, a carrier concentration of $\sim 4.38 \times 10^{17} cm^{-3}$. This values is in good agreement with the experimental reported value of approximately $-460\,\mu VK^{-1}$ at 300 K for $Mg_2Si_{0.3}Sn_{0.7}$ [38]. The highest S value for p-type behavior is 549.14 μVK^{-1} at a carrier concentration of 5.91×10^{17} cm^{-3}. With increase in T at any carrier concentration, S decreases due to an increase in charge carriers. With an increase in carrier concentration, the electrical conductivity also increases shifting the peak values of the PF and $S^2\sigma$ to higher μ as compared to that of S. The highest PF for n-type conduction is 3.03 mW m^{-1} K^{-2}, corresponding to μ of 0.24 eV, at carrier concentration of 1.99×10^{20} cm^{-3}. The maximum PF obtained is comparable to theoretical reported PF of 2.83 mW m^{-1} K^{-2} at 800 K with a carrier concentration 2.1×10^{20} cm^{-3} for $Mg_2Si_{0.25}Sn_{0.75}$ [39]. This also lies in the experimentally reported range of $\sim$3–4 mW m^{-1} K^{-2} from 350 to 750 K for $Mg_2Si_{0.4}Sn_{0.6}$ [40]. The highest values of PF for p-type charge carriers is 2.78 mW m^{-1} K^{-2} for μ of 0.18 eV, at carrier concentration of 1.82×10^{20} cm^{-3}. ZT determines the efficiency or the device performance which, as evident in Fig. 4, does not correspond to the maxima position in PF. The maximum ZT values for n-type and p-type carriers are 0.56 (similar to 0.55 reported for n-type carrier at 700 K) [39] and 0.63 for carrier concentrations of 8.93×10^{19} and 9.04×10^{19} cm^{-3}, respectively, at $T = 600$ K. As observed from the HSE06 dispersion (Fig. S2 of the Supplemental Material [35]), $Mg_2Si_{0.296}Sn_{0.704}$ is an intrinsic semiconductor. Thus, at higher temperatures, the bipolar component of thermal conductivity starts to increase rapidly, decreasing the ZT values, as in the figure.

Small amount of Bi doping ($\sim$2%) at Si site has been reported to increase the electrical conduction [14]. As pointed out in Sec. III A, Bi doping have negligible contribution to the states near the band edges (VBM and CBM). This is quite interesting because it means Bi provides an extra free electron, thus increasing the electrical conduction (n-type) and at the same time does not affect the Seebeck coefficient values significantly. But slight change in S is observed due to the change in band topology caused by the hybridization of Bi atoms with its neighboring atoms. The μ dependence of S, PF, and ZT for $Mg_2Si_{0.296}Sn_{0.666}Bi_{0.037}$ at various temperatures is shown in Fig. 5. Clearly, small increase in S values as compared to that of n-type $Mg_2Si_{0.296}Sn_{0.704}$ is observed. The maximum S for n-type conduction is $-636.06\,\mu VK^{-1}$ corresponding to a carrier concentration of 4.92×10^{20} cm^{-3}. Because of an increase in carrier concentration with Bi doping, increases in

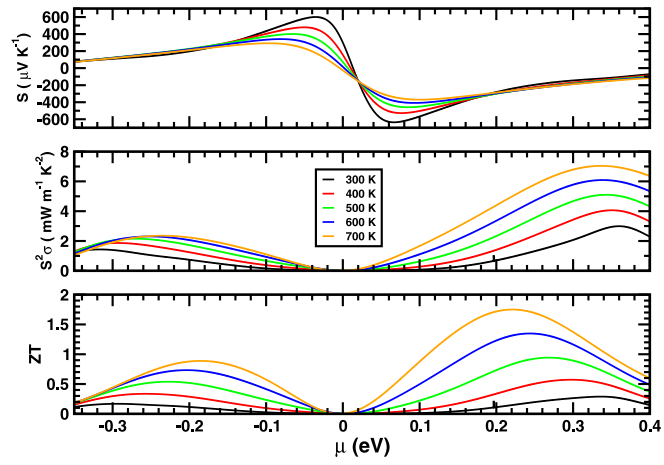

FIG. 5. Seebeck coefficient (S), power factor ($S^2\sigma$), and ZT vs μ at T's for $Mg_2Si_{0.296}Sn_{0.666}Bi_{0.037}$.

σ and hence the PF are observed for n-type conduction. The peak PF for n-type conduction is 7.04 mW m^{-1} K^{-2} at $\mu = 0.34$ eV corresponding to a carrier concentration of 7.77×10^{20} cm^{-3}. Bi doping increases the charge carriers, shifting the Fermi energy into the conduction bands, making the compound a degenerate semiconductor. This drastically suppress the bipolar thermal conductivity component as compared to that observed in the intrinsic semiconductor $Mg_2Si_{0.296}Sn_{0.704}$ for the concerned temperature range (as evident in Fig. S1), eventually enhancing the ZT values. However, it is important to note that the bipolar component will become important at higher temperatures when the concentration of the minority carriers becomes significantly large. Along with the increased PF for n-type conduction, the maximum ZT value we calculated is 1.75 at $\mu = 0.22$ eV corresponding to carrier concentration of 5.57×10^{20} cm^{-3}. This enhanced ZT is in agreement with previous experiments that reported values of 1.55 (773 K) [41], 1.2 (850 K) [42], and 1.4 (800 K) [43] for $Mg_{2.08}Si_{0.37}Sn_{0.6}Bi_{0.03}$, $Mg_2Si_{0.57}Sn_{0.4}Bi_{0.03}$, and $Mg_{2.16}Si_{0.388}Sn_{0.582}Bi_{0.03}$, respectively. This is an extremely promising result and begs an experimental confirmation.

The maximum value of S for p-type conduction is 600.55 μVK^{-1} at carrier concentration of 4.91×10^{20} cm^{-3}. In contrast, a decrease in maximum PF (2.35 mW m^{-1} K^{-2}) at carrier concentration of 4.33×10^{20} cm^{-3} is observed for Bi-doped compound as compared to $Mg_2Si_{0.296}Sn_{0.704}$. Because of the decrease in lattice thermal conductivity and absence of the bipolar component of κ (see Sec. II of the Supplemental Material [35]), the overall ZT for Bi-doped compound is higher than others. Maximum ZT for p-type conduction is found to be 0.88 at carrier concentration of 4.64×10^{20} cm^{-3}.

The effect of Cr doping on TE performance of Mg_2Si is yet to be explored. There are some studies of Cr-doping in MnS_2, and they show an enhancement of electrical conductivity and decrease in S with the increase of Cr content in the sample [22,23]. The increase in conductivity can be explained by the fact that Mn with $3d^5 4s^2$ valence electrons in $MnSi_2$ behaves as electron-deficient species which, when further doped with Cr (valence electrons $3d^5 4s^1$), increases the hole concentration, making it a better p-type conductor. A collective effect of electrical and thermal transport causes a small reduction in ZT with increasing amounts of Cr doping [23].

Here we have studied the TE performance of $Mg_{1.981}Cr_{0.019}Si_{0.296}Sn_{0.666}Bi_{0.037}$, where small amounts of Cr (replacing 1 Mg atom by Cr in a $3 \times 3 \times 3$ supercell) are doped into $Mg_2Si_{0.296}Sn_{0.666}Bi_{0.037}$. As shown in Fig. 6, a small decrease in the maximum S values is observed for both n-type and p-type conduction as compared to Mg_2(Si, Sn, Bi) case. This decrease is due to the lifting of degeneracy in band structure as observed in Fig. 3 (bottom). Maximum n-type S is $-616.94\,\mu$VK^{-1} at a carrier concentration of 4.97×10^{20} cm^{-3}, whereas the maximum p-type S is 543.54 μVK^{-1} at a carrier concentration of 4.96×10^{20} cm^{-3}. A reduction in PF is observed for both n-type and p-type charge carriers. The peak PF for n-type conduction is 4.33 mW m^{-1} K^{-2} at $\mu = 0.62$ eV with a carrier concentration of 4.76×10^{21} cm^{-3} while for p-type conduction, the peak PF is 1.52 mW m^{-1} K^{-2} at $\mu = -2.03$ eV and carrier concentration of 2.50×10^{22}cm^{-3}. Note that the peak value of these power factors are out of range of chemical potential

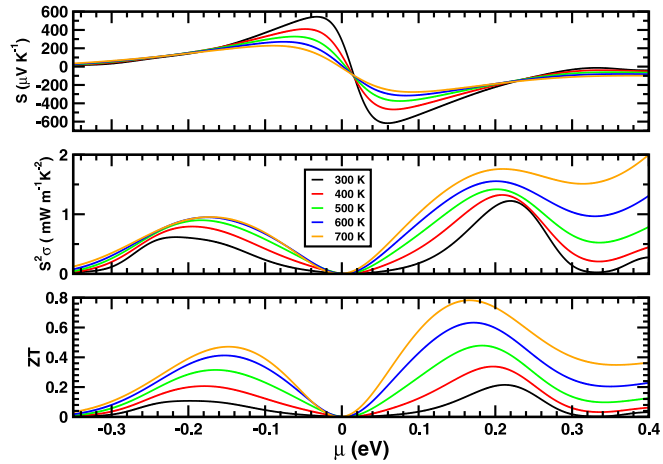

FIG. 6. S, $S^2\sigma$, and ZT vs μ at T's for $Mg_{1.981}Cr_{0.019}Si_{0.296}Sn_{0.666}Bi_{0.037}$.

values shown in Fig. 6. The peak ZT in this case, however, is smaller compared to the previous case. ZT for n-type and p-type carriers are 0.78 and 0.47, respectively, corresponding to a carrier concentration of 6.25×10^{20} cm^{-3} ($\mu = 0.17$ eV) and 3.86×10^{20} cm^{-3} ($\mu = 0.15$ eV). This is mainly due to the small decrease in the S and significant decrease in σ causing an overall reduction in ZT.

As shown in Figs. 4, 5, and 6, the optimal μ value (hence optimal carrier concentration) at each temperature, where the PF and ZT become maximum, are different. Now, maximizing PF is relevant when the maximum power/voltage ratio is required. Optimal carrier concentration where ZT is maximum, however, is more important, because ZT determines the TE efficiency. We, therefore, have chosen this optimal concentration and plotted the temperature dependence of S, $S^2\sigma$, and ZT in Fig. 7. The left (right) panel shows the result for n-type (p-type) carrier, where data for alloying with Sn (circles), Sn + Bi (squares), and Sn + Bi + Cr (triangles) are given. The $(ZT)_{max}$ values and the corresponding optimal values of T, n, S, $S^2\sigma$, and σ are listed in Table III.

The Seebeck coefficient at moderate temperature can be estimated as

$$S = \frac{\pi^2 k_B^2 T}{3eh^2} m^* \left(\frac{\pi}{3n}\right)^{2/3}, \tag{5}$$

where k_B, h, e, T, m^*, and n are the Boltzmann constant, Planck constant, electronic charge, temperature, carrier effective mass (in units of electron mass), and carrier concentration, respectively. With a fixed n, the S value increases with temperature as clearly evident from Fig. 7, for both n-type and p-type conduction. Optimal carrier concentration increases by an order of magnitude (10^{19} to 10^{20}) as we go from $Mg_2Si_{0.296}Sn_{0.704}$ to $Mg_2Si_{0.296}Sn_{0.666}Bi_{0.037}$ and $Mg_{1.981}Cr_{0.019}Si_{0.296}Sn_{0.666}Bi_{0.037}$ due to extra charge carriers provided by Bi. This results in highest PF of 5 mWm^{-1} K^{-2} observed for $Mg_2Si_{0.296}Sn_{0.666}Bi_{0.037}$. We note that the Cr doping decreases the TE performance of the Bi-doped compound. This can be explained by the small decrease in S accompanied by a large reduction in σ. Figure 8 shows the temperature dependence of σ for the three systems for both

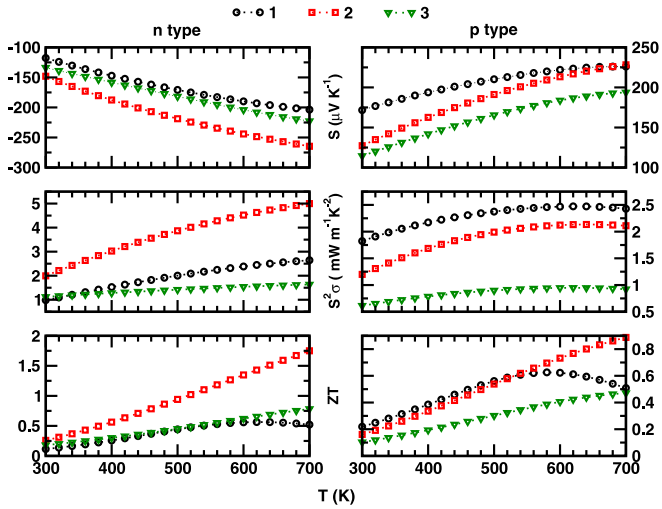

FIG. 7. Temperature dependence of Seebeck coefficients (S), power factor ($S^2\sigma$), and ZT for three systems. Here 1, 2, and 3 denote the $Mg_2Si_{0.296}Sn_{0.704}$, $Mg_2Si_{0.296}Sn_{0.666}Bi_{0.037}$, and $Mg_{1.981}Cr_{0.019}Si_{0.296}Sn_{0.666}Bi_{0.037}$, respectively. Optimal carrier concentration for compounds 1, 2, and 3 are 8.93×10^{19} cm^{-3}, 5.57×10^{20} cm^{-3}, and 6.25×10^{20} cm^{-3} for n-type carriers, and 9.05×10^{19} cm^{-3}, 4.64×10^{20} cm^{-3}, and 3.87×10^{20} cm^{-3} for p-type carriers, respectively.

n-type and p-type conduction. Clearly, a significant decrease in σ is found with Cr doping. Previous reports have suggested the role of Cr to act like a acceptor when doped at Mn site in the manganese silicides [22,23]. Because the valence shell of Cr is composed of $3d^5\,4s^1$ electrons and the total charge around Cr atom was found to be 5, it is clear that only one electron takes part in chemical bonding whereas the rest of the five are localized. Because one more electron is required to bind with the surrounding Sn and Si atoms, Cr atoms act as electron acceptor and, hence, decrease the conductivity. This, in turn, results in the decreased TE performance of $Mg_{1.981}Cr_{0.019}Si_{0.296}Sn_{0.666}Bi_{0.037}$.

IV. DISCUSSION

Doping $Mg_2Si_{0.296}Sn_{0.666}Bi_{0.037}$ with Cr was done by replacing a Mg atom by Cr in a $3 \times 3 \times 3$ supercell of the three-atom primitive cell. This gives a uniform sparse distribution of Cr atoms within the lattice. This, however, suppresses

TABLE III. Simulated maximum ZT values obtained for the three compounds for both n- and p-type conduction and the corresponding optimal $T(K)$, n ($\times 10^{20}$ cm^{-3}), S (μV K^{-1}), $S^2\sigma$ (mW m^{-1} K^{-2}), and σ (S cm^{-1}).

System	Doping type	T	n	S	$S^2\sigma$	σ	$(ZT)_{max}$
1	n	620	.893	−193.08	2.45	656.01	0.56
	p	580	.905	219.99	2.46	508.17	0.63
2	n	700	5.57	−264.61	5.0	714.03	1.75
	p	700	4.64	226.06	2.13	416.53	0.89
3	n	700	6.25	−222.65	1.63	329.36	0.78
	p	700	3.87	193.49	0.93	246.64	0.47

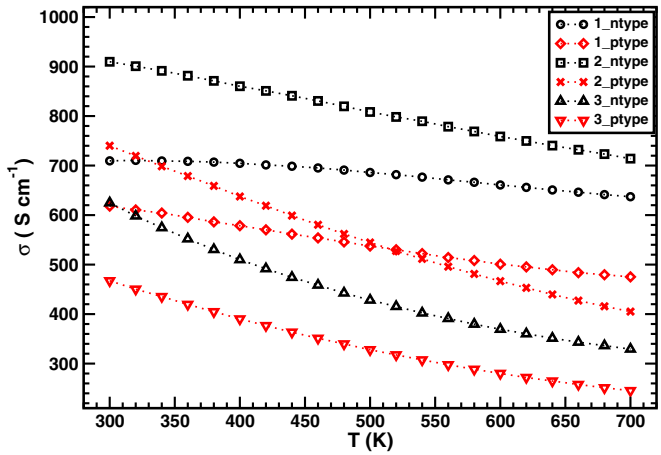

FIG. 8. σ vs T for $Mg_2Si_{0.296}Sn_{0.704}$, $Mg_2Si_{0.296}Sn_{0.666}Bi_{0.037}$, and $Mg_{1.981}Cr_{0.019}Si_{0.296}Sn_{0.666}Bi_{0.037}$ denoted by 1, 2, and 3, respectively. σ values are plotted for carrier concentration (n) at which ZT attains a maxima. The n values are mentioned in Table III.

the enhancements in TE performance that was gained by Bi doping. As mentioned earlier, Cr has antiferromagnetic spin density wave configuration in an elemental state which may lead to interesting properties. In our present system, there is one Cr atom sitting in a matrix of 54 Mg sites. This Cr atom is found to show almost negligible magnetic moment and thus non-spin-polarized calculation was performed. However, the influence of magnetism with the slight increase of Cr concentration and/or the spatial distribution of Cr in the given lattice can play a crucial role in dictating the TE performance.

To explore other stable configurations of Cr doping into the lattice, the energetics of various Cr doping (1.85, 3.7, 5.55, 7.4, 9.26, 11.11, and 12.96% Cr) in various magnetic orderings in the $Mg_{2-x}Cr_xSi$ is simulated. For 1.85% Cr, only one Cr atom is present in the $3 \times 3 \times 3$ supercell of the three-atom primitive cell. As a result, only nonmagnetic and ferromagnetic ordering can be studied for 1.85% Cr doping. In this case, the DFT energies of both the configurations have a negligible difference, with ferromagnetic ordering being slightly more stable. For other amounts of Cr ($>$1.85), different magnetic ordering states are shown in Fig. 9. Various abbreviations are used to denote different magnetic states with near or far distributions of Cr atoms. There are two important points which emerge from Fig. 9. First, the ferromagnetic configuration is the most stable order despite Cr being antiferromagnetic in its elemental state; $\geqslant$9.26% doping is a concentration where the energetics trend changes, still keeping the ferromagnetic ordering the most stable configuration. Second, as far as the effect of spatial distribution of the Cr atoms in the lattice is concerned, there can be two possibilities: (i) accumulation of Cr atoms in a certain region in the lattice and (ii) uniform distribution of Cr atoms spread out in the lattice. Depending on the size of the unit cell, we have simulated the energetics for these two possibilities, where in one case, Cr atoms were placed as far distance as possible from each other, and in the other case, they are placed near to each other (clustering), as labeled by -F and -N, respectively, in Fig. 9. The position of Cr atoms in the $3 \times 3 \times 3$ supercell for far (near) configurations are also shown in top (bottom) panel of

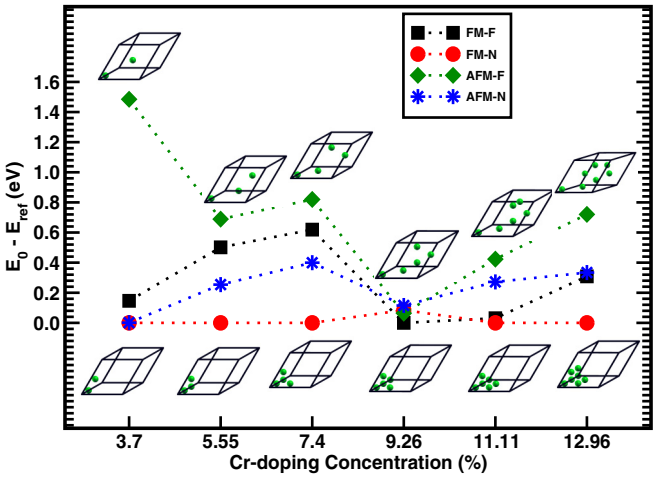

FIG. 9. Relative DFT formation energies of various amounts of Cr in Mg_2Si in different magnetic ordered states. The reference energy (E_{ref}) for each amount of Cr is chosen to be different from others to keep the most stable magnetic configuration for a particular level of Cr at lowest energy (0 eV). Abbreviations: FM-F, ferromagnetic far; FM-N, ferromagnetic near; AFM-F, antiferromagnetic far; and AFM-N, antiferromagnetic near. A schematic diagram of the near and far configurations for each level of Cr (showing only Cr atoms) is shown at the bottom and top, respectively.

Fig. 9 for each concentration. Looking at the energetics for these two cases for any given magnetic ordering, it is obvious that Cr atoms are energetically favored to stick close to each other in the lattice. This points toward the clustering of Cr atoms in the structure. Such clustering of atoms is expected to enhance the TE properties of the concerned material by reducing the lattice thermal conductivity due to scattering.

V. CONCLUSION

A systematic electronic-structure-based study of dispersion, band gap, and thermoelectric properties with selective alloying (large amounts of Sn and small amounts of Bi and Cr) in Mg_2Si was carried out. With careful combination of doping, a thermoelectric figure of merit (ZT) as high as 1.75 is achieved. $Mg_2Si_{0.296}Sn_{0.704}$ is found to be an indirect band gap (0.27 eV) semiconductor with Sn majorly contributing to the valence band edge. Small amount of Bi doping (3.7%) in the compound enhances the band gap to 0.33 eV but pushes the Fermi energy into the conduction band making it a degenerate semiconductor. With small Cr doping at Mg site, $Mg_{1.981}Cr_{0.019}Si_{0.296}Sn_{0.666}Bi_{0.037}$ maintains the band gap value (0.33 eV) but lifts the degeneracy of the low-lying conduction bands.

Bi-doping enhances the carrier concentration by an order of magnitude. Thus, in turn, enhances the TE properties, giving a ZT value of 1.75 at 700 K for n-type conduction as compared to $(ZT)_{max} = 0.56$ for n-type with only a Sn-doped sample. The corresponding Seebeck coefficient, power factor (PF), and optimal carrier concentration for Bi-doped compound are found to be $-265\,\mu VK^{-1}$, 5.0 mW m^{-1} K^{-2}, and 5.57 $\times 10^{20}$ cm^{-3}, respectively. ZT for p-type Bi-doped compound is 0.89. Interestingly, Cr doping in the (Sn + Bi) system diminishes the TE performance, giving a $(ZT)_{max}$ of 0.78 for n-type carrier. This is attributed to the decrease in S value due to the lifting of low-lying conduction band degeneracy and also a decrease in electronic conductivity σ.

A careful simulation of various magnetic and spatial configuration of Cr atoms suggests that Cr atoms energetically favor to align ferromagnetically and tend to cluster as opposed to having a uniform spatial distribution. In other words, they do not like to mix and must have a low solubility limit in the actual Cr-doped sample, if prepared in the laboratory. This clustering of Cr atoms is an advantage for very low Cr concentrations where the electrical conductivity is weakly affected by magnetic scattering. Such an agglomeration of any atom in a lattice structure helps to enhance the phonon scattering, which, in turn, reduces the lattice thermal conductivity. Simulating such clustered Cr doping requires an extremely large supercell and is beyond the scope of the present article. However, checking the same effect in a laboratory should not be nontrivial. We propose to prepare this compound and characterize it experimentally to shed some light on the present findings.

ACKNOWLEDGMENTS

Vikram acknowledges financial support from Indian Institute of Technology, Bombay in the form of teaching assistantship. A.A. acknowledges the National Centre for Photovoltaic Research and Education (NCPRE) (financially supported by Ministry of New Renewable Energy, MNRE, Government of India) for support of this research. A.A. also acknowledges useful discussions with T. Dasgupta on the transport data. D.D.J.'s support is from Iowa State University and the U.S. Department of Energy (DOE), Office of Science, Basic Energy Sciences, Materials Science and Engineering Division. His research was performed at Iowa State University (ISU) and Ames Laboratory, which is operated by ISU for the U.S. DOE under Contract No. DE-AC02-07CH11358.

[1] T. M. Tritt, Science **272**, 1276 (1996).
[2] T. M. Tritt, Science **283**, 804 (1999).
[3] F. J. DiSalvo, Science **285**, 703 (1999).
[4] D. Y. Chung, T. H. Hogan, P. Brazis, M. Rocci-Lane, C. Kannewurf, M. Bastae, C. Uher, and M. G. Kanatzidis, Science **287**, 1024 (2000).
[5] R. T. Littleton, Terry M. Tritt, J. W. Kolis, and D. R. Ketchum, Phys. Rev. B **60**, 13453 (1999).
[6] G. S. Nolas, M. Kaeser, and T. M. Tritt, Appl. Phys. Lett. **77**, 1855 (2000).
[7] B. C. Sales, D. Mandrus, and R. K. Williams, Science **272**, 1325 (1996).

[8] A. L. Pope, T. M. Tritt, M. A. Chernikov, and M. Feuerbacher, Appl. Phys. Lett. **75**, 1854 (1999).

[9] V. K. Zaitsev, M. I. Fedorov, E. A. Gurieva, I. S. Eremin, P. P. Konstantinov, Y. A. Samunin, and M. V. Vedernikov, Phys. Rev. B **74**, 045207 (2006).

[10] V. K. Zaitsev, M. I. Fedorov, I. S. Eremin, and E. A. Gurieva, in *Thermoelectric Handbook, Macro to Nano*, edited by D. M. Rowe (CRC Press, Oxon, UK, 2006), Chaps. 29 and 31.

[11] K. Kishida, A. Ishida, T. Koyama, S. Harada, N. L. Okamoto, K. Tanaka, and H. Inui, Acta Mater. **57**, 2010 (2009).

[12] W. H. Luo, H. Li, Y. G. Yan, Z. B. Lin, X. F. Tang, Q. J. Zhang, and C. Uher, Intermetallics **19**, 404 (2011).

[13] H. Wang, W. Chu, and H. Jin, Comput. Mater. Sci. **60**, 224 (2012).

[14] J.-C. Tani and H. Kido, Physica B (Amsterdam, Neth.) **364**, 218 (2005).

[15] Q. Zhang, X. Su, Y. Yan, H. Xie, T. Liang, Y. You, X. Tang, and C. Uher, ACS Appl. Mater. Interfaces **8**, 3268 (2016).

[16] K. Yin, X. Su, Y. Yan, Y. You, Q. Zhang, C. Uher, M. G. Kanatzidis, and X. Tang, Chem. Mater. **28**, 5538 (2016).

[17] A. S. Tazebay, S.-I. Yi, J. K. Lee, H. Kim, J.-H. Bahk, S. L. Kim, S.-D. Park, H. S. Lee, A. Shakouri, and C. Yu, ACS Appl. Mater. Interfaces **8**, 7003 (2016).

[18] W. Liu, X. Tang, H. Li, J. Sharp, X. Zhou, and C. Uher, Chem. Mater. **23**, 5256 (2011).

[19] H. Balout, P. Boulet, and M.-C. Record, J. Phys. Chem. C **118**, 19635 (2014).

[20] D. Cederkrantz, N. Farahi, K. A. Borup, B. B. Iversen, M. Nygren, and A. E. C. Palmqvist, J. Appl. Phys. **111**, 023701 (2012).

[21] X. Cheng, N. Farahi, and H. Kleinke, J. Minerals, Metals and Materials Society **68**, 2680 (2016).

[22] T. Nakamura, K. Yoshioka, R. Arai, J.-ichi Nishioka, M. Hirakawa, K. Fujimoto, R. Tamura, and K. Nishio, MRS Adv. **3**, 1367 (2018).

[23] G. Liu, Q. Lu, X. Zhang, J. Zhang, and Y. Shi, J. Electron. Mater. **41**, 6 (2012).

[24] P. Hohenberg and W. Kohn, Phys. Rev. **136**, B864 (1964).

[25] G. Kresse and J. Furthmüller, Comput. Mater. Sci. **6**, 15 (1996).

[26] G. Kresse and J. Furthmüller, Phys. Rev. B **54**, 11169 (1996).

[27] G. Kresse and J. Hafner, Phys. Rev. B **47**, 558 (1993).

[28] P. E. Blöchl, Phys. Rev. B **50**, 17953 (1994).

[29] J. P. Perdew, K. Burke, and M. Ernzerhof, Phys. Rev. Lett. **77**, 3865 (1996).

[30] A. V. Krukau, O. A. Vydrov, A. F. Izmaylov, and G. E. Scuseria, J. Chem. Phys. **125**, 224106 (2006).

[31] P. E. Blöchl, O. Jepsen, and O. K. Andersen, Phys. Rev. B **49**, 16223 (1994).

[32] G. K. H. Madsen and D. J. Singh, Comput. Phys. Commun. **175**, 67 (2006).

[33] H.-S. Kim, Z. M. Gibbs, Y. Tang, H. Wang, and G. J. Snyder, APL Mater. **3**, 041506 (2015).

[34] T. Dasgupta *et al.* (unpublished).

[35] See Supplemental Material at http://link.aps.org/supplemental/10.1103/PhysRevB.98.115204 for (i) description of method to extract the carrier relaxation time (τ), (ii) the experimental lattice thermal conductivity data, and (iii) the HSE06 dispersion on a sparse set of k-points.

[36] K. Kutorasiński, J. Tobola, and S. Kaprzyk, Phys. Rev. B **87**, 195205 (2013).

[37] J.-H. Bahk, Z. Bian, and A. Shakouri, Phys. Rev. B **89**, 075204 (2014).

[38] Y. Z. Zhang, Y. H. Han, and Q. S. Meng, Mater. Res. Innovations **19**, 264 (2015).

[39] X. J. Tan, W. Liu, H. J. Liu, J. Shi, X. F. Tang, and C. Uher, Phys. Rev. B **85**, 205212 (2012).

[40] A. Sankhla, A. Patil, H. Kamila, M. Yasseri, N. Farahi, E. Mueller, and J. de Boor, ACS Appl. Energy Mater. **1**, 531 (2018).

[41] P. Gao, X. Lu, I. Berkun, R. D. Schmidt, E. D. Case, and T. P. Hogan, Appl. Phys. Lett. **105**, 202104 (2014).

[42] G. S. Polymeris, N. Vlachos, E. Symeou, and T. Kyratsi, Phys. Status Solidi A **215**, 1800136 (2018).

[43] W. Liu, Q. Zhang, K. Yin, H. Chi, X. Zhou, X. Tang, and C. Uher, J. Solid State Chem. **203**, 333 (2013).